Orbital characters and near two-dimensionality of Fermi surfaces in $NaFe_{1-x}Co_xAs$

Cite as: Appl. Phys. Lett. **101**, 202601 (2012); https://doi.org/10.1063/1.4767374
Submitted: 08 April 2012 • Accepted: 30 October 2012 • Published Online: 13 November 2012

Z.-H. Liu, P. Richard, Y. Li, et al.

Orbital characters and near two-dimensionality of Fermi surfaces in $NaFe_{1-x}Co_xAs$

Z.-H. Liu,[1] P. Richard,[2] Y. Li,[1] L.-L. Jia,[1] G.-F. Chen,[1] T.-L. Xia,[1] D.-M. Wang,[1] J.-B. He,[1] H.-B. Yang,[3] Z.-H. Pan,[3] T. Valla,[3] P. D. Johnson,[3] N. Xu,[2] H. Ding,[2] and S.-C. Wang[1,a)]
[1]*Department of Physics, Renmin University, Beijing 100872, People's Republic of China*
[2]*Beijing National Laboratory for Condensed Matter Physics and Institute of Physics, Chinese Academy of Sciences, Beijing 100190, China*
[3]*Condensed Matter Physics and Materials Science Department, Brookhaven National Laboratory, Upton, New York 11973, USA*

(Received 8 April 2012; accepted 30 October 2012; published online 13 November 2012)

We report a comprehensive study of orbital characters and tridimensional nature of the electronic bands of 111-family in Fe-pnictides superconductors, $NaFe_{1-x}Co_xAs$ ($x = 0$ and 0.05), with angle-resolved photoemission spectroscopy. We determined the orbital characters and the k_z dependence of the low-energy electronic structures by tuning the polarization and the energy of the incident photons. We observed two nearly two-dimensional hole-like Fermi surfaces (FS) near the Brillouin zone (BZ) center and two electron-like FS near BZ corner. The bands near the Fermi level (E_F) are mainly derived from the Fe $3d_{xy}$, $3d_{yz}$, and $3d_{zx}$ orbitals. © *2012 American Institute of Physics*. [http://dx.doi.org/10.1063/1.4767374]

The pairing mechanism of the superconductivity in Fe-based superconductors (IBSC) had been a central debate ever since the discovery of IBSC with T_c as high as 56 K.[1,2] Interband scattering was proposed as pairing glue based on the observation of quasi-nesting condition between electron-like Fermi surfaces (FS) and hole-like FS in the most known four families of IBSC, namely "1111," "122," "111," and "11" families.[1–5] However, there have been reports of the absence of hole-like FS in the recently discovered $A_yFe_{2-x}Se_2$ (A = K, Rb, Cs, Tl, etc.),[6–9] which exhibit a superconducting transition temperature (T_c) of about 30 K.[10,11] The lack of hole-FS casts doubt on interband scattering or FS nesting as an essential ingredient for the unconventional superconductivity in IBSC.

Orbital dependency of electron bands was proposed to explain the superconductivity in IBSC.[12,13] Theoretically, it has been proposed that the FS sheets with multiple orbitals could result in a strong anisotropy and amplitude variation of the superconducting gaps.[14,15] Experimentally, a study on 122-family shows that the superconducting gap sizes are different at the same Fermi momentum for two bands with different orbital symmetries.[16] To construct the correct models for IBSC, and to understand the unconventional superconductivity, it is thus critical to experimentally identify the orbital characters of low-energy electronic structure. In this report, we experimentally identify the orbital characters of low-energy electronic structure in the 111-family, i.e., $NaFe_{1-x}Co_xAs$.

The 111-family of Fe-pnictides is an ideal candidate for angle-resolved photoemission spectroscopy (ARPES) study due to its non-polar cleaved surface. Recent ARPES work on cobalt doped $NaFe_{1-x}Co_xAs$[17] has reported sharp quasiparticle features compared with other Fe-pnictides families. Here we report a detailed ARPES study on $NaFe_{1-x}Co_xAs$ ($x = 0$ and 0.05) using differing photon polarizations and energies to identify the orbital characters and k_z dependence of the bands. We observed two hole-like FS near the Brillouin zone (BZ) center and two electron-like FS near the BZ corner. The bands near E_F are hybridizations of the Fe $3d_{xy}$, $3d_{yz}$, and $3d_{zx}$ orbitals and have weak k_z dispersion. Away from E_F, we also observed a band located at 230 meV below E_F from the Fe $3d_{z^2}$ orbital, with a strong k_z dispersion.

High quality single crystals were synthesized by the flux method. Samples with cross sectional area $1 \times 1\,mm^2$ were mounted in a gas protected glove box to prevent reaction with moisture and were cleaved *in situ* yielding flat mirror-like (001) surfaces. ARPES measurements were performed at Renmin University of China and Institute of Physics (China Academic of Science) using a Scienta R4000 analyzer with He-discharge lamp (He-Iα line, $h\nu = 21.2$ eV), the Synchrotron Radiation Center, WI, Apple-PGM beamline with Scienta 200U analyzer, and the Beamline U13B of National Laboratory of Light Source, NY, with a Scienta 2002. During measurements, the pressure was maintained below 5×10^{-11} Torr. No noticeable aging was observed during each measurement cycle. The E_F was referenced to the leading edge of a fresh Au thin film in good electrical contact to the sample, and the overall energy resolution was better than 12 meV.

The BZ of $NaFe_{1-x}Co_xAs$ and high symmetry points are presented in Fig. 1(d). By changing the incident photons energy ($h\nu$), one can probe the band dispersion along the c-axis with different k_z's. The k_z values can be determined empirically by the formula[18]

$$k_z = \sqrt{\frac{2m}{\hbar^2}[(h\nu - \phi - E_b)\cos^2\theta + V_0]}, \qquad (1)$$

where $h\nu$ is the photon energy, ϕ the work function, V_0 the inner potential of the sample, and θ the emission angle of photoelectrons relative to the sample's surface normal.

a)Electronic mail: scw@ruc.edu.cn.

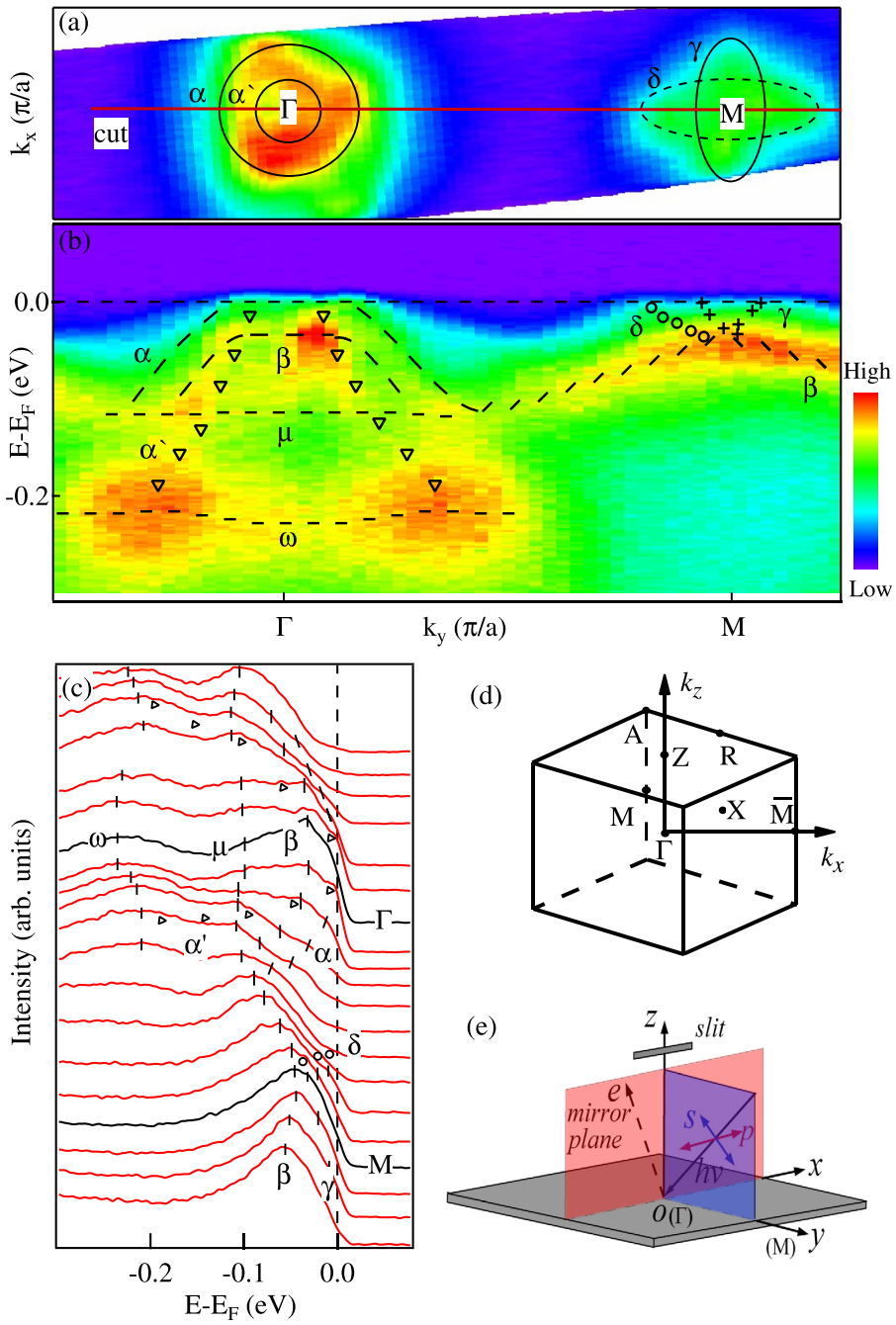

FIG. 1. ARPES data along ΓM direction with photon energy 21.2 eV, He-discharge lamp, T = 20 K. (a) Integrated intensity map as FS of NaFeAs, integrated within ±10 meV with respect to E_F. α′ is obscured by the inner of the two circles drawn around Γ. (b) Intensity plots of band dispersion along ΓM direction, indicated as cut in (a). (c) The energy distribution curves (EDCs) plot for the data in panel (b). (d) BZ of NaFeAs and high symmetry points. (e) Experimental geometry setup for polarization dependent measurement. The electric field of *p* polarized light is primarily along the *x* direction, and the *s* polarized light along *y* direction, and contains a *z*-component.

The intensity of each band is dominated by the matrix element (photon excitation probability) which depends on symmetry of the band, the polarization of the incident photons, and their relative angle. The linear polarization of the photons can be exploited in two different experimental geometries (*p* and *s*), as shown in Fig. 1(e). In the ARPES experiment, the high-symmetry direction and the normal of the sample surface define a mirror plane. The *p* (*s*) polarization experimental geometry refers to the electric fields of the incident photons within (normal to) the mirror plane respectively. Assuming the final-state of the outgoing electron depicted by a plane wave, the wave function ϕ_f^k remains even with respect to the plane.[19] The matrix element is described by

$$|M_{f,i}^k|^2 \propto |\langle \phi_f^k | \vec{\varepsilon} \cdot \vec{r} | \phi_i^k \rangle|^2, \quad (2)$$

where $\vec{\varepsilon} \cdot \vec{r}$ describes the relative arrangement between the incident photon polarization and the outgoing electron direction. When $\vec{\varepsilon} \cdot \vec{r}$ is even (odd), only the even (odd) component of the initial state ϕ_i^k could be detected.[20] We define the *x*-axis along the Fe-Fe direction (Γ-$\bar{M}$ in *k* space). Thus the $d_{x^2-y^2}$, d_{z^2}, and d_{zx} are of even symmetry, while the d_{xy} and d_{yz} are of odd symmetry with respect to Γ$\bar{M}$ plane. In our experimental setup, the angle of separation between incoming photon beam direction and the axis of the spectrometer is about 50°. Thus the *s* polarized light contains a *z*-component of electric field (ε_z), as sketched in Fig. 1(e). The d_{z^2} orbital is noticeably enhanced in *s* geometry due to this *z*-component.[21]

Fig. 1(a) shows the FS map of NaFeAs at T = 20 K using non-polarized He-discharge lamp. Two hole-like FS are observed at Γ point, named as α and α′, respectively, and two electron-like FS are observed at M point, named as γ(δ),

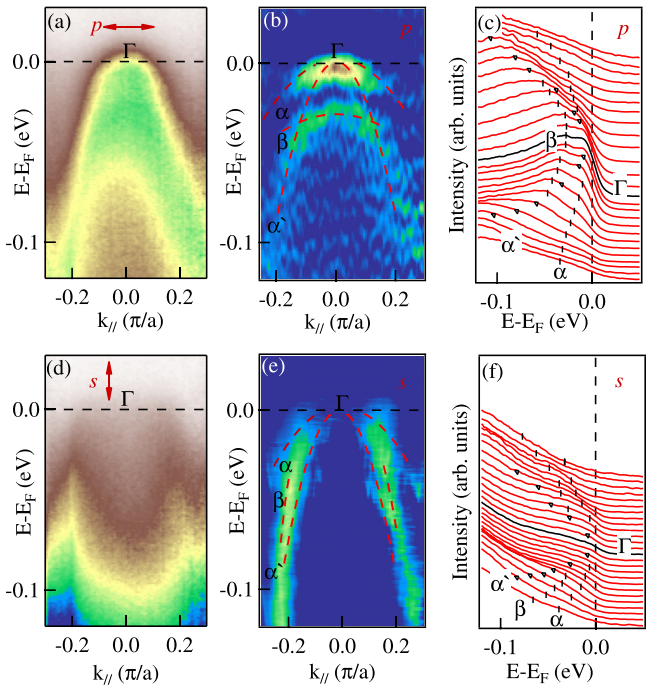

FIG. 2. The ARPES data around Γ along Γ$\bar{M}$ direction with the linearly polarized light and photon energy hν = 36 eV at T = 20 K. (a) Intensity plot taken at Γ point in *p* geometry. (b) Second derivative $[\partial^2 I(\omega,k)/\partial\omega^2]$ intensity plot of data in panel (a) to illustrate the band dispersion. (c) EDCs of the data in panel (a). The markers are band dispersions plotted as guide to the eye. (d)-(f) The same as panels (a), (b), and (c), respectively, but taken in *s* geometry. The electric fields are indicated by arrows in (a) and (d).

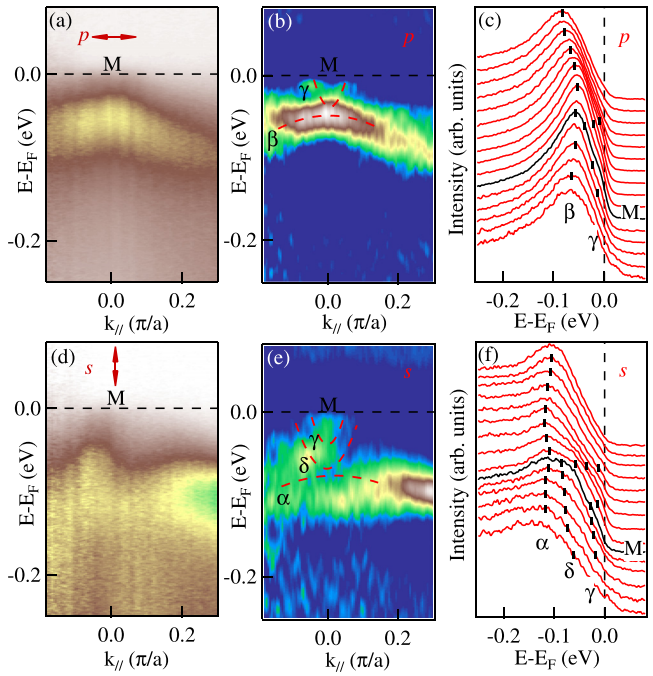

FIG. 3. The ARPES data around M along Γ$\bar{M}$ direction with the linearly polarized light and photon energy hν = 36 eV at T = 20 K. (a) Intensity plot taken at M point in *p* geometry. (b) Second derivative $[\partial^2 I(\omega,k)/\partial\omega^2]$ intensity plot of data in panel (a) to illustrate band dispersion. (c) EDCs for the data in panel (a). The markers are band dispersions plotted as guide to the eye. (d)-(f) The same as panels (a), (b), and (c), respectively, but taken in *s* geometry. The electric fields are indicated by arrows in (a) and (d).

while the δ FS is a 90° rotation of γ FS and will be clearly identified by the polarized light. The bands dispersion of NaFeAs along the ΓM direction is shown in Figs. 1(b) and 1(c). At Γ point, we can identify five bands below E_F, named as α, β, α', μ, and ω, respectively. The α and α' bands cross the E_F, forming two hole-like FS, labeled correspondingly in Fig. 1(a). The α band is within the vicinity of 120 meV from E_F, while the α' band extended up to 200 meV in binding energy. The two bands should be degenerate at the Γ point above E_F, due to the crystal having C_4 symmetry. The β band lies between α and α' below E_F and cross α', exhibiting a flat top at 30 meV below E_F. The μ and ω bands locate at about 120 meV and 230 meV below E_F, respectively. At the M point are two electron-like bands, $\gamma(\delta)$ crossing E_F with band minima at 30 meV below E_F and form two electron-like FS centered around M. All the observations are in agreement with LDA band structure calculations.[22]

To identify the parity of each band, we use different polarizations of the linearly polarized light source. As Figs. 2 and 3 show, the polarization dependent data taken along the Γ$\bar{M}$ direction with *p* and *s* polarized light have clear differences. In the *p* geometry the even orbitals with respect to the Γ$\bar{M}$ mirror plane get enhanced, while the odd orbitals are suppressed, and vice-versa for *s* geometry. Figs. 2(a)–2(c) and 2(d)–2(f) show the photoemission intensity around Γ point in *p* and *s* geometry, respectively. From the figures, the top of β band is greatly enhanced in *p* geometry, as shown in Fig. 2(c), and is fully suppressed in *s* geometry, as shown in Fig. 2(f), while the tail of the β band exhibits an opposite behavior, which suggests a complex symmetry of the β band. The α' band shows high intensity and is clearly identifiable in the *p* geometry, as shown in Fig. 2(c), remaining visible in the *s* geometry but with much weaker intensity, as shown in Fig. 2(f). The intensity of α band does not visibly change between *p* and *s* geometries. All three bands can be seen in both geometries, which means that the β, α', and α bands are mixed with the orbitals of opposite symmetries.

Fig. 3 shows the polarization dependence of the data around M point. Compared with the bands around Γ, the orbital components of each band is less mixed around M point. In the *p* geometry, the β band is greatly enhanced, with the bottom located at about 100 meV below E_F, and the α band is greatly suppressed. The γ band is also clearly observed with its bottom around 30 meV below E_F, while the δ band is fully suppressed. In the *s* geometry, the α, δ, and γ band are observable, while the β band is suppressed.

According to the LDA band structure calculations,[22–24] the bands close to E_F are mainly from the Fe $3d_{xy}$, $3d_{yz}$, and $3d_{zx}$ orbitals, and they are greatly hybridized. The summary of each bands intensity response to the *p*, *s* geometries, the symmetry of the bands and the possible combination of orbitals are listed in Table I. Note that the d_{yz} and d_{zx} are degenerate at the Γ point due to the crystal having C_4 symmetry. The α band crosses E_F and is seen in both the *p*, *s* geometries, and thus it should be mixture of d_{xy}, d_{yz}, and d_{zx} orbitals. The α' band is enhanced in both geometries, so it should be the hybridization of the d_{xy}, d_{yz}, and d_{zx} orbitals. The β band crosses with the α' band at binding energy of 30 meV and is separated into two parts. The top of β band is enhanced in the *p* geometry and suppressed in the *s* geometry, so it contains only the orbital with even symmetry, i.e., d_{zx} orbital, while the rest β band exhibits an opposite behavior, so it contains mainly the odd orbitals, i.e., d_{xy} or d_{yz}.

TABLE I. The summary of orbital components of each bands close to E_F and its parity. "+/−" represents the band intensity enhanced/suppressed in the corresponding geometry.

k point	Bands name	*p*	*s*	Orbitals	Parity
Γ	α	+	+	d_{xy} d_{yz} d_{zx}	Mixed
	α′	+	+	d_{xy} d_{yz} d_{zx}	Mixed
	β top	+	−	d_{zx}	Even
	β tail	−	+	d_{xy} d_{yz}	Odd
M	α	−	+	d_{xy} d_{yz}	Odd
	β	+	−	d_{zx}	Even
	γ	+	+	d_{xy} d_{yz} d_{zx}	Mixed
	δ	−	+	d_{xy} d_{yz}	Odd

In comparison to the Γ point, the bands at the M point are more identifiable. The β band is even with respect to $\bar{M}\Gamma$ plane which mainly contains the d_{zx} orbital. The γ band has no visible change between the *p* and *s* geometries, and it contains orbitals with both even (d_{zx}) and odd (d_{xy} and d_{yz}) geometries. The α and δ bands can only be seen in the *s* geometry; thus, they should contain only orbitals of odd character (d_{xy} or d_{yz}).

To study the three-dimensional character of the electronic structure, we conducted a photon energy dependence measurement on NaFeAs and $NaFe_{0.95}Co_{0.05}As$, using the *s* polarized light and the right circularly polarized light (RC). At a fixed in-plane momentum, data measured with different photon energies correspond to different k_z, as in Eq. (1). As Figs. 4(a) and 4(b) show, we measured the k_z dispersion of $NaFe_{0.95}Co_{0.05}As$ from 30 eV to 76 eV which covers the Z-Γ-Z in k_z. The ω band at about 230 meV below E_F is strongly dispersive along k_z. The LDA calculations predict a strong k_z dispersion of the Fe $3d_{z^2}$ orbital sinking to high binding energy at the Γ point.[22–24] Thus, the main contribution to the ω band is by the Fe $3d_{z^2}$ orbital. The μ band has no noticeable k_z dispersion, and its intensity changes dramatically with the photon energy, being greatly enhanced at Z. A similar behavior has been observed in Co-doped $BaFe_2As_2$ system,[25] whose origin and the orbital character need further study.

According to Eq. (1), with empirical value of inner potential 10.3 eV, and periodicity of $2\pi/c' = 0.894$ Å, with $c' = c/2 = 7.028$ Å (due to bilayer FeAs),[4] we found that 21, 44, and 70 eV are close to the Γ point, while 32 and 56 eV are close to the Z point. Fig. 4(a) shows the α and α′ FS in the $k_{\|}$-k_z plane; both bands have noticeable k_z dispersion. The rate of Fermi momentum change (R) along k_z direction, $R = (k_{\|\Gamma}\text{-}k_{\|Z})/k_{\|\Gamma} \approx 27\%$, is much less than that of the 122-family, which was reported to have a much more three-dimensional FS with $R \approx 70\%$ in electron-doped $BaFe_{1-x}Co_xAs_2$.[25,26] From the observation of 122-family, the description of superconductivity and magnetism in pnictides have to consider the orbital-dependent 3D electronic structure. The weaker magnetism and lower T_c in the 111-family could be related to the weaker three dimensionality. Finally, more detailed measurements of the k_z dispersion from 34 to 48 eV of NaFeAs is compared with $NaFe_{0.95}Co_{0.05}As$. As shown in Fig. 4(d), the α′ and β band dispersion along k_z are still weak, the μ band has almost no k_z dispersion, and the ω band strongly disperses along k_z.

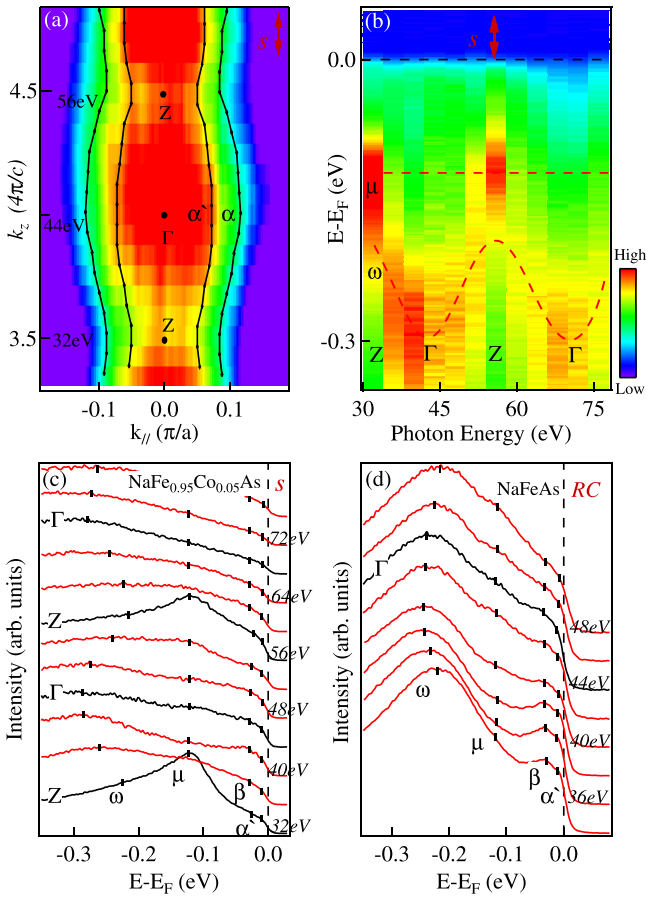

FIG. 4. The photon energy dependent ARPES data taken at 20 K. (a) Integrated intensity plot as FS of $NaFe_{0.95}Co_{0.05}As$ in the $k_{\|}$-k_z plane, using the *s* polarized light. The line served as guide to the eye of FS of α and α′. (b) Intensity plot taken along k_z direction, corresponding (a). The line served as guide to the eye of band μ and ω. (c) EDCs for the data in panel (b). (d) EDCs of NaFeAs in more detailed measurements from 34 to 48 eV, using the RC.

There is no difference between the Co-doped and parent samples except the shift of the chemical potential due to Co-substitution which carries extra electron to the system.

In summary, we analyzed the orbital character and the k_z dispersion in $NaFe_{1-x}Co_xAs$, by carrying out the polarization and photon energy dependent ARPES. The bands near Fermi level are mixtures of the orbitals with opposite symmetries, indicating strong hybridization of orbitals. Photon energy dependent experimental data reveal a strong k_z dispersion around −230 meV, and the dispersion of the low energy bands with k_z is weaker than that in 122-family, forming near two-dimensional FS. Additionally the nonpolar surface and comparatively sharply quasi-particle feature in the electron-doped sample indicates that this is a good two-dimensional system for studying IBSC.

This work was supported by the grants from the Chinese Academy of Sciences, the Ministry of Science and Technology of China, the National Science Foundation of China, the Fundamental research Funds for the central university and the Research Funds of RUC. The National Synchrotron Light Source is supported by the US Department of Energy. The Synchrotron Radiation Center, Stoughton (WI) is supported by the National Science Foundation under Award No. DMR-0537588.

[1]Y. Kamihara, T. Watanabe, M. Hirano, and H. Hosono, J. Am. Chem. Soc. **130**, 3296 (2008).
[2]Z. A. Ren, J. Yang, W. Lu, W. Yi, G. C. Che, X. L. Dong, L. L. Sun, and Z. X. Zhao, Mater. Res. Innovations **12**, 105 (2008).
[3]M. Rotter, M. Tegel, D. Johrendt, I. Schellenberg, W. Hermes, and R. Pöttgen, Phys. Rev. B **78**, 020503(R) (2008).
[4]G. F. Chen, W. Z. Hu, J. L. Luo, and N. L. Wang, Phys. Rev. Lett. **102**, 227004 (2009).
[5]F. C. Hsu, J. Y. Luo, K. W. Yeh, T. K. Chen, T. W. Huang, P. M. Wu, Y. C. Lee, Y. L. Huang, Y. Y. Chu, D. C. Yan, and M. K. Wu, Proc. Natl. Acad. Sci. **105**, 14262 (2008).
[6]T. Qian, X.-P. Wang, W.-C. Jin, P. Zhang, P. Richard, G. Xu, X. Dai, Z. Fang, J.-G. Guo, X.-L. Chen, and H. Ding, Phys. Rev. Lett. **106**, 1870012 (2011).
[7]Y. Zhang, L. X. Yang, M. Xu, Z. R. Ye, F. Chen, C. He, H. C. Xu, J. Jiang, B. P. Xie, J. J. Ying, X. F. Wang, X. H. Chen, J. P. Hu, M. Matsunami, S. Kimura, and D. L. Feng, Nat. Mater. **10**, 273 (2011).
[8]D. X. Mou, S. Y. Liu, X. W. Jia, J. F. He, Y. Y. Peng, L. Zhao, L. Yu, G. D. Liu, S. L. He, X. L. Dong, J. Zhang, H. D. Wang, C. H. Dong, M. H. Fang, X. Y. Wang, Q. J. Peng, Z. M. Wang, S. J. Zhang, F. Yang, Z. Y. Xu, C. T. Chen, and X. J. Zhou, Phys. Rev. Lett. **106**, 132502 (2011).
[9]Z.-H. Liu, P. Richard, N. Xu, G. Xu, Y. Li, X.-C. Fang, L.-L. Jia, G.-F. Chen, D.-M. Wang, J.-B. He, T. Qian, J.-P. Hu, H. Ding, and S.-C. Wang, Phys. Rev. Lett. **109**, 037003 (2012).
[10]J. G. Guo, S. F. Jin, G. Wang, S. C. Wang, K. X. Zhu, T. T. Zhou, M. He, and X. L. Chen, Phys. Rev. B **82**, 180520 (2010).
[11]D. M. Wang, J. B. He, T.-L. Xia, and G. F. Chen, Phys. Rev. B **83**, 132502 (2011).
[12]T. D. Stanescu, V. Galitski, and S. D. Sarma, Phys. Rev. B **78**, 195114 (2008).
[13]T. Shimojima, F. Sakaguchi, K. Ishizaka, Y. Ishida, T. Kiss, M. Okawa, T. Togashi, C.-T. Chen, S. Watanabe, M. Arita, K. Shimada, H. Namatame, M. Taniguchi, K. Ohgushi, S. Kasahara, T. Terashima, T. Shibauchi, Y. Matsuda, A. Chainani, and S. Shin, Science **332**, 564 (2011).
[14]F. Wang, H. Zhai, and D. H. Lee, Phys. Rev. B **81**, 184512 (2010).
[15]R. Thomale, C. Platt, W. Hanke, and B. A. Bernevig, Phys. Rev. Lett. **106**, 187003 (2011).
[16]Y. Zhang, L. X. Yang, F. Chen, B. Zhou, X. F. Wang, X. H. Chen, M. Arita, K. Shimada, H. Namatame, M. Taniguchi, J. P. Hu, B. P. Xie, and D. L. Feng, Phys. Rev. Lett. **105**, 117003 (2010).
[17]Z.-H. Liu, P. Richard, K. Nakayama, G.-F. Chen, S. Dong, J.-B. He, D.-M. Wang, T.-L. Xia, K. Umezawa, T. Kawahara, S. Souma, T. Sato, T. Takahashi, T. Qian, Y.-B. Huang, N. Xu, Y.-B. Shi, H. Ding, and S.-C. Wang, Phys. Rev. B **84**, 064519 (2011).
[18]S. Hüfner, *Photoelectron Spectroscopy* (Springer-Verlag, Berlin, 1995), p. 354.
[19]J. Hermanson, Solid State Commun. **88**, 1097 (1993).
[20]A. Damascelli, Z. Hussain, and Z.-X. Shen, Rev. Mod. Phys. **75**, 473 (2003).
[21]X.-P. Wang, P. Richard, Y.-B. Huang, H. Miao, L. Cevey, N. Xu, Y.-J. Sun, T. Qian, Y.-M. Xu, M. Shi, J.-P. Hu, X. Dai, and H. Ding, Phys. Rev. B **85**, 214518 (2012).
[22]K. Kusakabe and A. Nakanishi, J. Phys. Soc. Jap. **78**, 124712 (2009).
[23]S. Q. Deng, J. Köhler, and A. Simon, Phys. Rev. B **80**, 214508 (2009).
[24]S. V. Borisenko, V. B. Zabolotnyy, D. V. Evtushinsky, T. K. Kim, I. V. Morozov, A. N. Yaresko, A. A. Kordyuk, G. Behr, A. Vasiliev, R. Follath, and B. Büchner, Phys. Rev. Lett. **105**, 067002 (2010).
[25]P. Vilmercati, A. Fedorov, I. Vobornik, U. Manju, G. Panaccione, A. Goldoni, A. S. Sefat, M. A. McGuire, B. C. Sales, R. Jin, D. Mandrus, D. J. Singh, and N. Mannella, Phys. Rev. B **79**, 220503 (2009).
[26]W. Malaeb, T. Yoshida, A. Fujimori, M. Kubota, K. Ono, K. Kihou, P. M. Shirage, H. Kito, A. Iyo, H. Eisaki, Y. Nakajima, T. Tamegai, and R. Arita, J. Phys. Soc. Jpn. **78**, 123706 (2009).